OMPS LP Observations of PSC Variability During the NH 2019-2020 Season

Matthew T. DeLand[1,2], Pawan K. Bhartia[2], Natalya Kramarova[2], Zhong Chen[1,2]

[1]Science Systems and Applications, Inc. (SSAI).

[2]NASA Goddard Space Flight Center, Code 614.

Corresponding author: Matthew DeLand (matthew.deland@ssaihq.com)

Key Points:

- Polar stratospheric clouds are a precursor to seasonal ozone depletion
- The OMPS Limb Profiler can create vertically resolved daily maps of PSC distribution
- The Arctic 2019-2020 winter/spring season had high PSC occurrence rates more typically observed in the Antarctic

Abstract

Seasonal ozone depletion in the polar regions (during late winter and early spring) depends on the presence and distribution of polar stratospheric clouds (PSCs). In this paper, we present new satellite observations of PSCs by the Ozone Mapping and Profiler Suite (OMPS) Limb Profiler (LP) instrument. LP cloud detections are identified as PSCs based on location, altitude, and background atmosphere temperature. The hyperspectral capabilities of OMPS LP enable PSC detection to occur concurrent with stratospheric ozone measurements from the same instrument. We present PSC results from the Northern Hemisphere 2019-2010 winter/spring season to illustrate the exceptional nature of this season. Future OMPS LP instruments flying on Joint Polar Satellite System (JPSS) satellites will continue PSC observations into the 2030s.

Plain Language Summary

The presence of polar stratospheric clouds is an important factor in determining whether polar ozone depletion occurs during the spring. We present new observations of PSCs from the OMPS Limb Profiler (LP), collected in parallel with ozone profile measurements by the same instrument. LP observations show that the Arctic 2019-2020 winter/spring season was exceptional in terms of PSC geographic coverage and duration. LP measurements of PSCs will continue with future satellite instruments.

1 Introduction

Seasonal depletion of stratospheric ozone layer in polar region is regularly observed in the Southern Hemisphere (SH) during late winter and early spring (August-October). A key component of this depletion comes from chemical reactions involving chlorine and bromine species that are sequestered on polar stratospheric cloud (PSC) surfaces during polar night. Active chlorine is then released through photodissociation of these species when sunlight returns in the spring (e.g. Solomon, 1991).

Corresponding levels of seasonal ozone depletion are much less common in the Northern Hemisphere (NH) polar region, and quite variable in magnitude. This difference is directly related to the less stable polar vortex in the NH due to surface topography generating gravity waves that disrupt the zonal flow (e.g. Waugh et al., 2017), which makes it more difficult to reach and maintain the cold temperatures needed for PSC formation. The observation and characterization of NH PSCs is thus a valuable precursor to estimating springtime NH ozone depletion.

The Northern Hemisphere 2019-2020 winter/spring season was exceptional in terms of PSC formation and longevity in the Arctic. This paper presents new observations of PSCs from the Ozone Mapping and Profiling Suite (OMPS) Limb Profiler (LP). We use the existing cloud detection algorithm of Chen et al. (2016) to identify clouds, and apply further criteria to discriminate PSCs from this population. We also estimate the depth of the PSC layer in order to provide an estimate of total PSC area for ozone depletion calculation. The LP PSC results are compared to a sample of CALIOP v2 PSC data for initial validation. Since LP PSC observations are coincident with ozone profiles retrieved from the same instrument, these PSC results provide a direct indication of the local conditions that lead to ozone depletion.

2 LP Instrument and Cloud Detection

The OMPS instruments (Nadir Mapper, Nadir Profiler, Limb Profiler) are designed to continue the long-term record of total column ozone and profile ozone (Flynn et al., 2009). The first set of OMPS instruments was launched on the Suomi National Polar-orbiting Partnership (S-NPP) satellite on 28 October 2011. The Limb Profiler (LP) uses limb scattering measurements to achieve good vertical resolution (~1.6 km) with continuous sampling along the orbit. LP views the atmosphere in a backward direction with three vertical slits, one aligned with the orbit track and the other two separated by ±4.25° horizontally. Use of a 2-D CCD detector provides hyperspectral data with altitude coverage between 0-80 km and wavelength coverage between 290-1000 nm. Jaross et al. (2014) gives a more extensive discussion of the LP instrument and its characteristics.

The LP cloud detection algorithm uses the difference of the vertical gradient in radiance between measurements at 675 nm and 869 nm, also termed radiance ratio, as defined by Chen et al. (2016). In the current Version 1.5 (V1.5) aerosol extinction product (Chen et al., 2018), the radiance ratio profile (RR) is calculated over the altitude range 5.5-40.5 km for each measurement (event), and the largest value of RR > 0.15 is reported as the cloud height z_{cloud}.

Since the LP cloud detection algorithm only indicates the presence of a cloud and does not provide other characteristics, we need additional tests to evaluate the possible classification of any detection as a PSC. We use ancillary meteorological data (provided with the LP V1.5 aerosol product) from the Global Modeling and Assimilation Office (GMAO) Forward Processing-Instrument Team (FP-IT) GEOS 5.12.4 assimilation processing (Gelaro et al., 2017), which are supplied at 0.5° latitude x 0.625° longitude sampling and 3-hour time steps. Since the FP-IT spatial grid is finer than the LP sampling separation, we select the nearest grid cell to each LP measurement, then interpolate data at the bracketing times to the time of the LP measurement. We use the interpolated temperature profile and tropopause altitude for PSC classification. In order to reduce the possibility of contamination by cirrus clouds in the polar region, we also require any PSC detection to have a cloud height at least 2 km above the local tropopause.

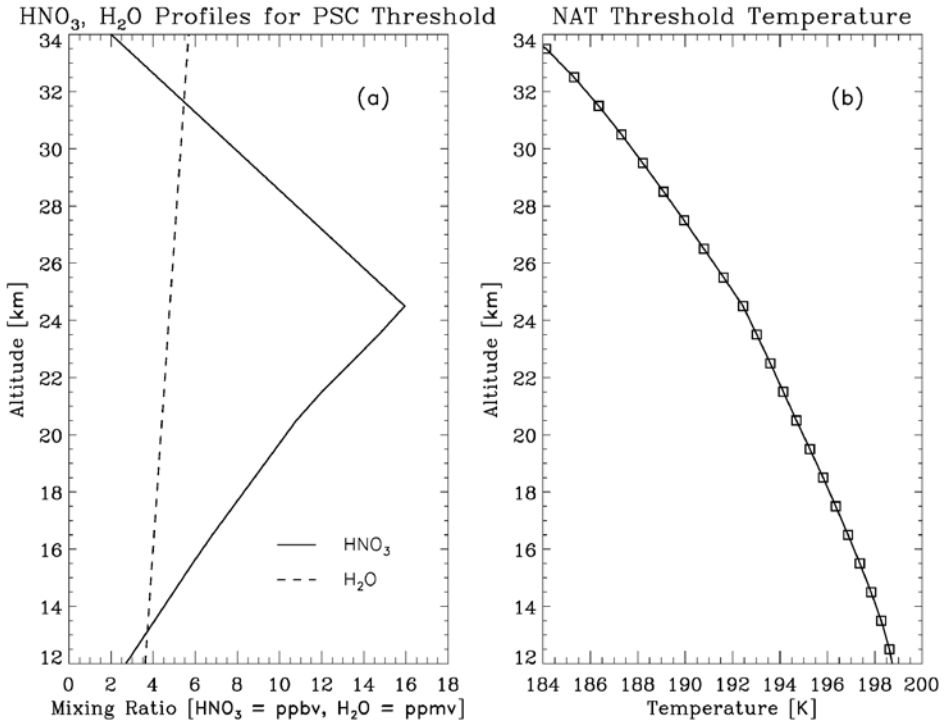

Figure 1. (a) Mixing ratio profiles of HNO_3 (*solid*) and H_2O (*dashed*) for use in calculating NAT formation threshold. (b) NAT formation temperature threshold for PSC classification in LP measurements.

The formation temperature for nitric acid trihydrate (NAT) particles found in Type I PSCs can be determined from the phase relationship given by Hanson and Mauersberger (1988). That relationship is a function of the partial pressure of HNO_3 and H_2O, which means that we need to specify the abundance of these species. We have constructed simplified mixing ratio profiles appropriate for high latitude winter/spring conditions based on the Microwave Limb Sounder (MLS) results of Santee et al. (2007) for HNO_3 and Lambert et al. (2007) for H_2O, as shown in Figure 1(a). The NAT temperature threshold profile [$T_{PSC}(z)$] calculated using these data is shown in Figure 1(b), and varies from ~200 K at 12 km to 187 K at 32 km. This profile is relatively insensitive to the specific mixing ratio values; reducing the HNO_3 profile by a factor of two only lowers $T_{PSC}(z)$ by ~1 K. We therefore use a single $T_{PSC}(z)$ threshold profile for all LP analysis presented in this paper.

3 LP PSC Results

Figure 2 shows OMPS LP PSC detection results for 3 December 2019. This is relatively early in the NH season to have a significant amount of PSC activity, based on the climatology of CALIOP PSC results shown by Pitts et al. (2018). The northernmost extent of PSC detection is significantly affected by the limitation of useful LP measurements to solar zenith angles < 88°, thus excluding polar night regions. PSCs are identified at altitudes between 20.5-26.5 km on this date, and only in a longitude region from ~90°E to 15°W. Such restricted geographic distribution has been ascribed to persistent patterns in planetary wave activity (e.g. Zhang et al., 2016).

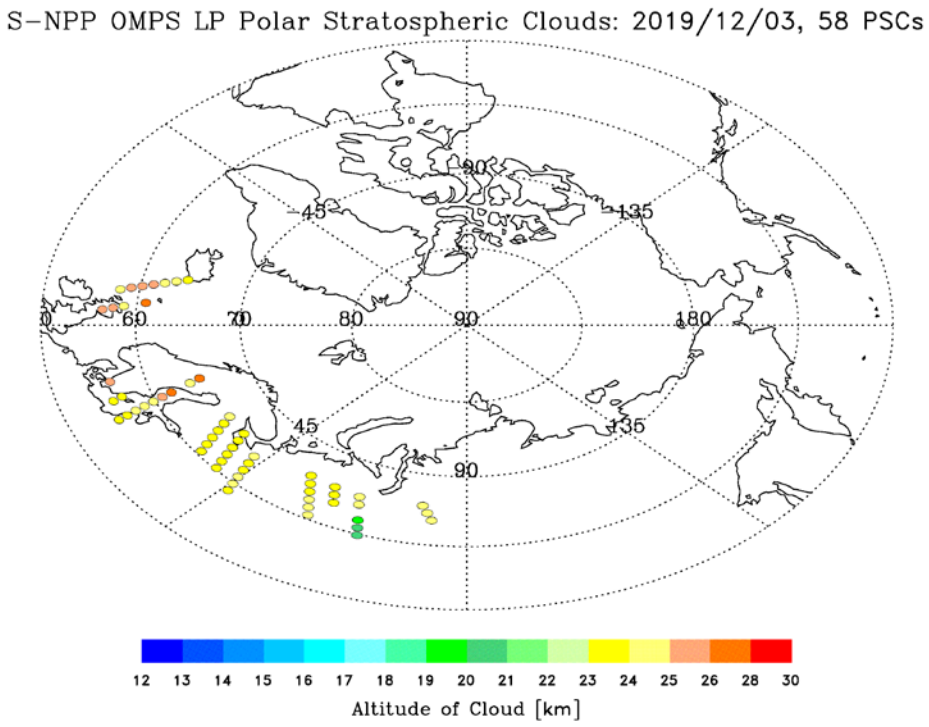

Figure 2. OMPS LP polar stratospheric cloud detection between 50°-90°N for 3 December 2019. Cloud altitudes are indicated by the color scale.

Figure 3 shows the LP PSC detection results for 9 March 2020. The CALIOP data record shows virtually no PSC activity at this time of year during the 11-year period 2006-2017, let alone the extensive activity shown here. PSC altitudes are lower in March (13.5-18.5 km in this example), and the longitudinal region covered by PSCs has shifted to span from ~90°E eastward to ~90°W. The latitude region of PSCs now extends up to ~82°N, reflecting the seasonal shift in LP viewing coverage.

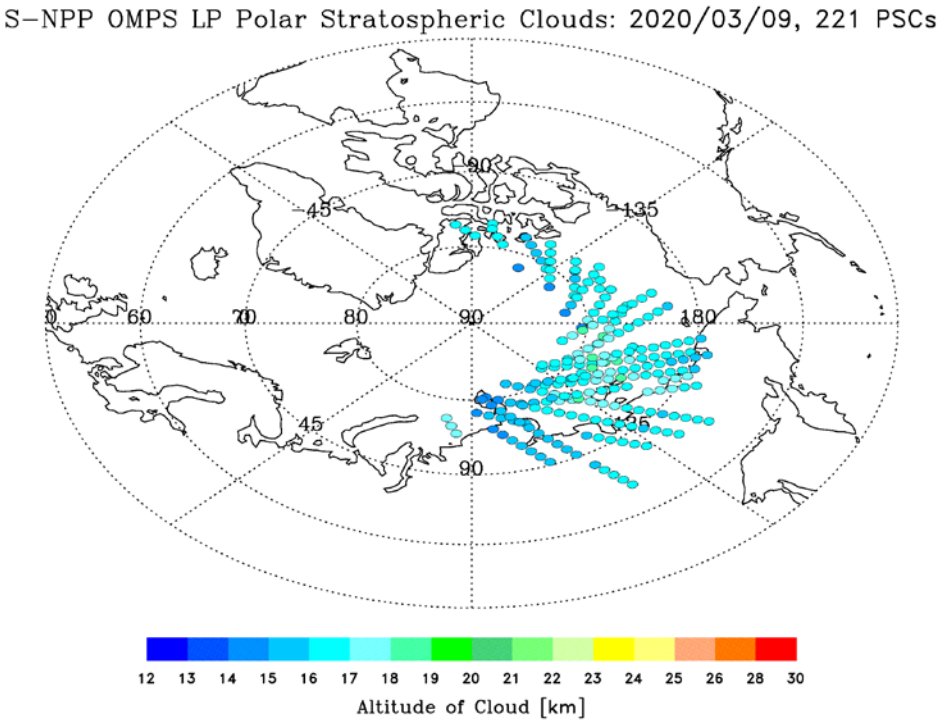

Figure 3. OMPS LP polar stratospheric cloud detection between 50°-90°N for 9 March 2020.

The influence of the LP viewing geometry on PSC observations is further illustrated in Figure 4, which shows LP PSC occurrence frequency in five equal area latitude bands between 50°-85° during the NH 2019-2020 season. The corresponding progression of the maximum latitude viewed by LP is shown in Figure 4(b). Note that the highest value is approximately 85°. Latitude bands up to 64.7°-71.8°N show modest and relatively constant behavior during the season, with daily frequency values (zonally averaged) reaching ~20%. In contrast, the 71.8°-85.0°N band quickly jumps to 30-40% frequency in early February, concurrent with the time when this latitude band first becomes visible to LP.

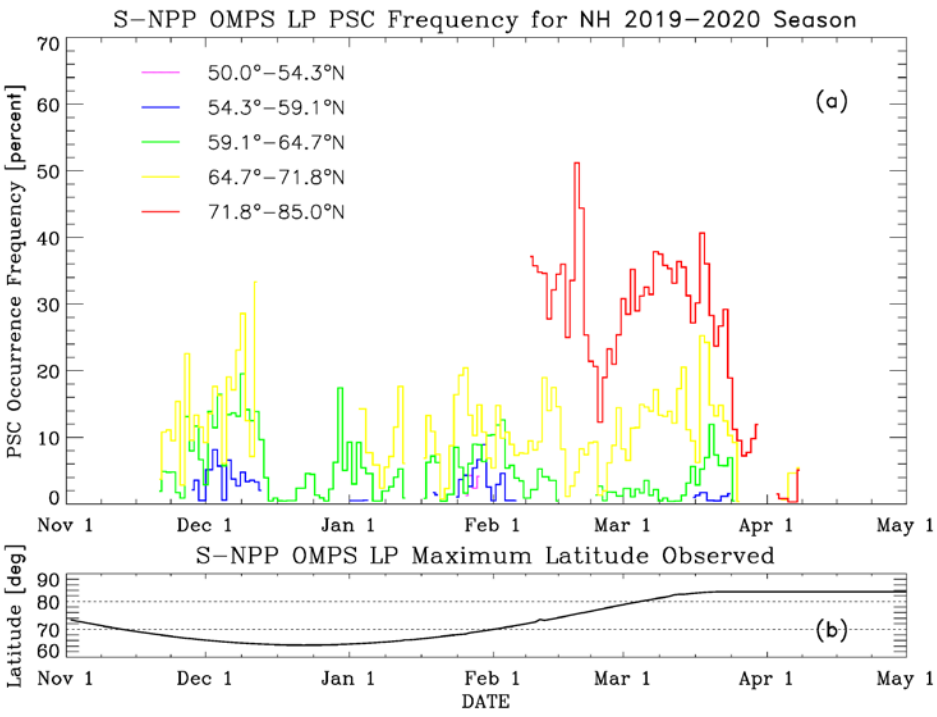

Figure 4. (a) LP PSC frequency in equal area latitude bands during the NH 2019-2020 season. (b) Maximum latitude observed by OMPS LP during the NH 2019-2020 season.

We would like to determine the area covered by PSCs at each altitude in order to estimate the potential magnitude of stratospheric ozone loss. Since LP only identifies the top of a PSC, we need to use an indirect approach. One method is to examine the temperature profiles below each cloud for additional levels where $T_{event}(z) < T_{PSC}(z)$. This "cold" layer can be up to 13 km thick in some cases. Figure 5 shows comparisons between the LP PSC area as a function of altitude for selected days, including additional cold layer levels as PSCs, and the total PSC area from CALIOP v2 data (Pitts et al., 2018) integrated over the latitude range visible to LP. PSC area is determined as the product of the daily PSC occurrence frequency in small latitude bands (~3°-4°) and the spatial area of each band. We find that using the full depth of the cold layer indicated by the ancillary temperature profile gives LP PSC areas that are significantly larger than CALIOP areas in the lower part of the stratosphere. This result seems unrealistic, since CALIOP area values at all altitudes are based on actual PSC detections. Testing different limits suggests that restricting the depth of the cold layer to $\Delta z \leq 7$ km gives a more appropriate result for LP PSC area estimates.

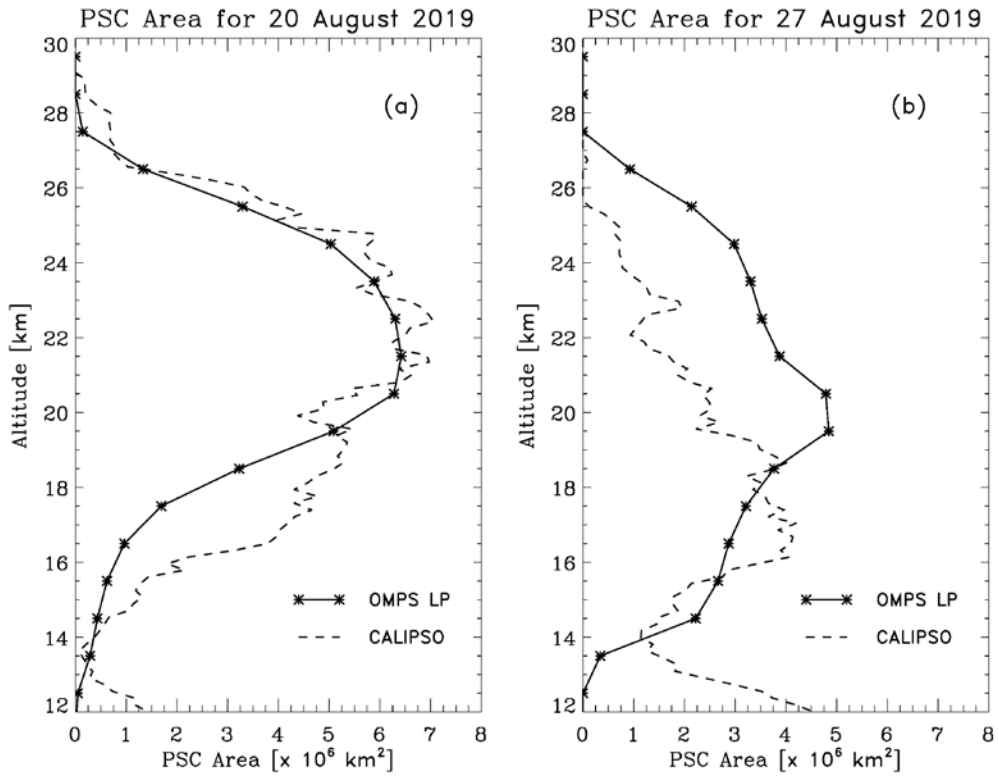

Figure 5. (a) Calculated PSC area as a function of altitude by OMPS LP (solid) and CALIOP (dashed) for 20 August 2019. For OMPS LP, all layers with T < T_{PSC} up to 7 km below the cloud altitude are considered in the PSC area calculation. CALIOP V2 data are limited to the LP latitude range. (b) Calculated PSC area for 27 August 2019. Definitions are as in part (a).

Figure 6 shows the time dependence of PSC area for the NH 2019-2020 season as calculated by OMPS LP, using the maximum layer thickness of 7 km as discussed. Area values of 2-3 million km^2 are seen at 22-27 km in early December, when LP spatial coverage of the NH polar region is lowest. PSC altitudes move down during the season, and area values increase in March 2020 to a maximum of > 10 million km^2 at 17-19 km. This is an exceptional result: CALIOP observations during 2005-2016 typically show almost no NH PSC activity in March, whereas PSC area values of 6-8 million km^2 observed in March 2020 are comparable to average mid-August PSC areas in the SH (Pitts et al., 2018).

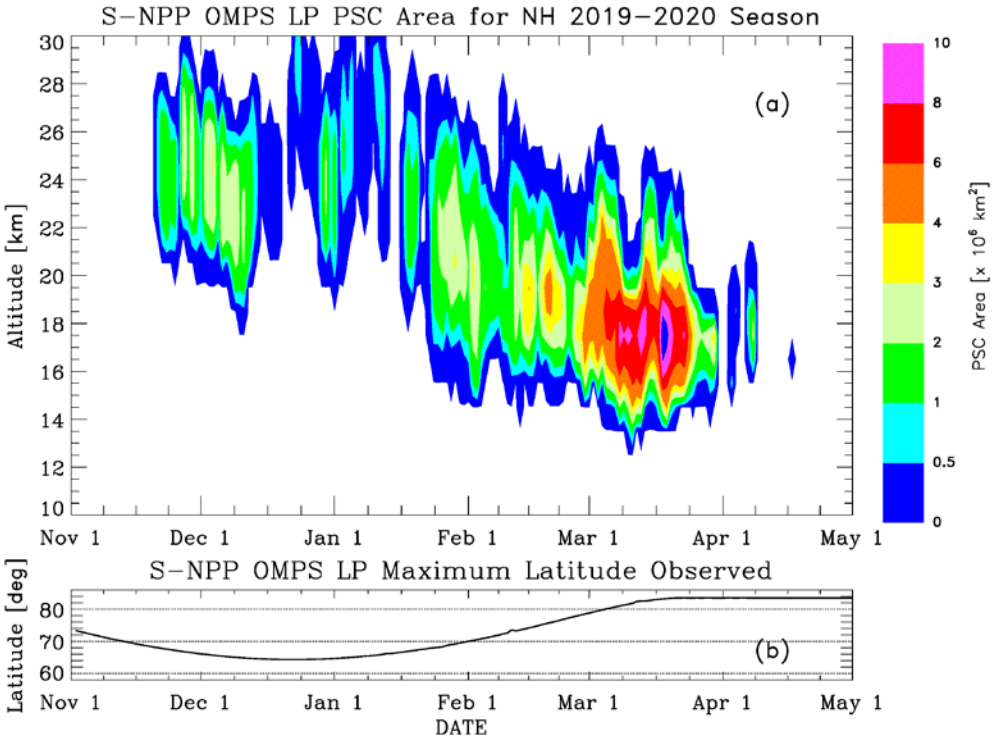

Figure 6. OMPS LP PSC area as a function of altitude during the NH 2019-2020 season, including all layers with $T < T_{PSC}$ up to 7 km below the cloud detection altitude. (b) Maximum latitude observed by OMPS LP during the NH 2019-2020 season.

The increased amount of PSCs during late winter and early spring of 2019-2020 led to unprecendented low ozone levels over the Arctic region. LP ozone measurements in March-April 2020 show severely depleted lower stratosphere (12.5-18.5 km) ozone concentrations (Figure 7), with a maximum decrease of -12 DU/km (or -50%) relative to the 2012-2019 average observed by LP in the same region. Ozone concentration values averaged over the polar cap region were as low as 6-8 DU/km, compared to typical values of 14-22 DU/km in the altitude region 12-25 km.

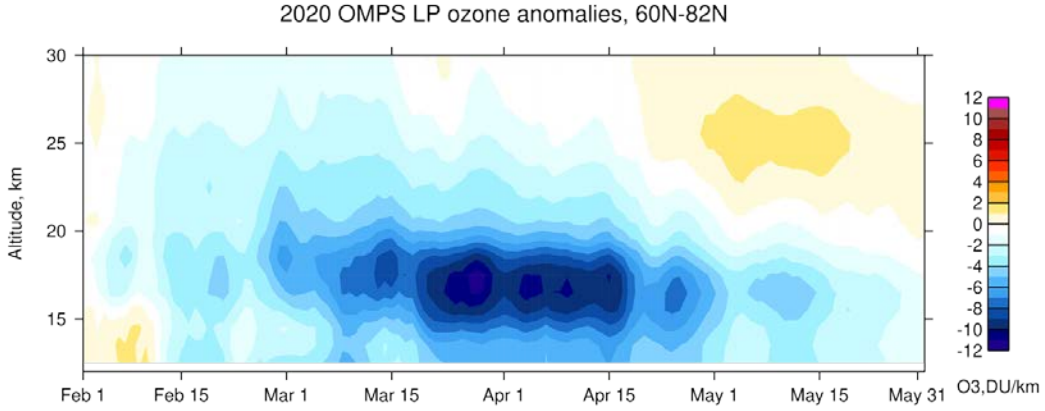

Figure 7. OMPS LP lower stratosphere ozone concentration depletion between 60°-82°N during February-May 2020. Differences are calculated relative to the LP average concentration observed during the period 2012-2019 for the same months and latitude range.

The return of sunlight to northern polar latitudes during February-April activated chlorine and bromine reactions on the surface of PSC particles that catalytically destroy ozone. The massive lower stratospheric Artic ozone depletion observed in 2020 is thus a direct result of photochemical processes. The magnitude of ozone loss is substantially larger than any previous year in the LP data record, which begins in April 2012. We note that while the LP algorithm does cut off individual ozone profile retrievals at the identified cloud top (Kramarova et al., 2018), ozone depletion also occurs in air masses that surround PSC locations. The longevity of the Arctic polar vortex in spring 2020, sustaining PSC conditions into early April (as shown in Figure 6), also prolonged the ozone depletion by preventing meridional transport of ozone-rich air from outside the polar region.

The magnitude of the spring 2020 Arctic ozone depletion is significantly greater than any biases or drifts identified in correlative studies of the LP ozone product (Kramarova et al., 2018). Since the difference results shown in Figure 7 are calculated relative to a multi-year average of LP data, any residual bias cancels out. While LP upper stratospheric ozone data do show a small drift relative to MLS data (believed to be caused by a drift in LP altitude registration), this effect has a negligible impact near the ozone profile peak at ~18 km. We have validated the results presented in this paper by examining quasi-coicident MLS ozone profiles for the same period.

4 Conclusions

Characterizing the frequency and location of polar stratospheric clouds is a valuable diagnostic tool for predicting possible short-term ozone depletion during polar spring conditions. We have shown that OMPS LP cloud detection results can be filtered to consistently identify PSCs in sunlit regions. LP PSC measurements are a valuable indicator for polar ozone chemistry because they capture the early spring conditions when substantial photochemical ozone loss occurs due to chlorine and bromine catalytic reactions. These measurements complement CALIOP PSC results that are based on nighttime data. Using co-located temperature profiles from assimilation products, we also calculate estimated PSC area as a function of altitude. The NH 2019-2020 season was remarkable in this respect, with maximum area values of 8-10 million km^2 in the lower stratosphere that are comparable to typical SH PSC values. We plan to extend our observational comparisons of LP ozone and PSC data back to the start of the LP data record in early 2012. Additional PSC information will be available when a second OMPS LP instrument is launched on the next Joint Polar Satellite System satellite (JPSS-2), currently scheduled for early 2022.

Acknowledgments and Data Access

Michael Pitts graciously provided sample CALIOP v2 PSC data prior to the full product release, as well as valuable guidance on interpretation of the LP PSC results.

OMPS LP V1.5 aerosol data, containing cloud detection information and ancillary temperature profiles, are available at the GES DISC: https://doi.org/10.5067/GZJJYA7L0YW2 (Bhartia and Torres, 2019).

References

Bhartia, P. K., & Torres, O. (2019). OMPS-NPP LP L2 Aerosol Extinction Vertical Profile swath daily 3slit V1.5, Greenbelt, MD, USA, Goddard Earth Sciences Data and Information Center (GES DISC), https://doi.org/10.5067/GZJJYA7L0YW2

Chen, Z., DeLand, M., & Bhartia, P. K. (2016). A new algorithm for detecting cloud height using OMPS/LP measurements. *Atmospheric Measurement Techniques*, *9*, 1239-1246, https://doi.org/10.5194/amt-9-1239-2016

Chen, Z., Bhartia, P. K., Loughman, R., Colarco, P., & DeLand, M. (2018). Improvement of stratospheric aerosol extinction retrieval from OMPS/LP using a new aerosol model. *Atmospheric Measurement Techniques*, *11*, 6495-6509, https://doi.org/10.5194/amt-11-6495-2018

Flynn, L. E., McNamara, D., Beck, C. T., Petrapavlovskikh, I., Beach, E., Pachepsky, Y., Li, Y. P., DeLand, M., Huang, L.-K., Long, C. S., Seftor, C. J., Tiruchirapalli, R., & Taylor, S. (2009). Measurements and products from the Solar Backscatter Ultraviolet (SBUV/2) and the Ozone Mapping and Profiler Suite (OMPS) instruments. *International Journal of Remote Sensing*, *30*, 4259-4272, https://doi.org/10.1080/01431160902825040

Gelaro, R., McCarty, W., Suárez, M. J., Todling, R., Molod, A., Takacs, L., Randles, C. A., Darmenov, A., Bosilovich, M. G., Reichle, R., Wargan, K., Coy, L., Cullather, R., Draper, C., Akella, S., Buchard, V., Conaty, A., da Silva, A. M., Gu, W., Kim, G., Koster, R., Lucchesi, R., Merkova, D., Nielsen, J. E., Partyka, G., Pawson, S., Putman, W., Rienecker, M., Schubert. S. D., Sienkiewicz, M., & Zhao, B. (2017). The Modern-Era Retrospective Analysis for Research and Applications, version 2 (MERRA-2). *Journal of Climate*, *30*, 5419-5454, https://doi.org/10.1175/JCLI-D-16-0758.1

Hanson, D. R., & Mauersberger, K. (1988). Laboratory studies of the nitric acid trihydrate: Implications for the south polar stratosphere. *Geophysical Research Letters*, *15*, 855-858, https://doi.org/10.1029/GL015i008p00855

Jaross, G., Bhartia, P. K., Chen, G., Kowitt, M., Haken, M., Chen, Z., Xu, P., Warner, J., & Kelly, T. (2014). OMPS Limb Profiler instrument performance assessment. Journal of Geophysical Research Atmospheres, 119, 4399-4412, https://doi.org/10.1002/2013JD020482

Kramarova, N. A., Bhartia, P. K., Jaross, G., Moy, L., Xu, P., Chen, Z., DeLand, M., Froidevaux, L., Livesey, N., Degenstein, D., Bourassa, A., Walker, K. A., & Sheese, P. (2018). Validation of ozone profile retrievals derived from the OMPS LP version 2.5 algorithm against correlative satellite measurements. Atmospheric measurement Techniques, 11, 2837-2861, https://doi.org/10.5194/amt-11-2837-2018

Lambert, A., Read, W. G., Livesey, N. J., Santee, M. L., Manney, G. L., Froidevaux, L., Wu, D. L., Schwartz, M. J., Pumphrey, H. C., Jiminez, C., Nedoluha, G. E., Cofield, R. E., Cuddy, D. T., Daffer, W. H., Drouin, B. J., Fuller, R. A., Jarnot, R. F., Knosp, B. W., Pickett, H. M., Perun, V. S., Snyder, W. V., Stek, P. C., Thurstans, R. P., Wagner, P. A., Waters, J. W., Jucks, K. W., Toon, G. C., Stachnik, R. A., Bernath, P. F., Boone, C. D., Walker, K. A., Urban, J., Murtagh, D., Elkins, J. W., & Atlas, E. (2007). Validation of the Aura Microwave Limb Sounder middle atmosphere water vapor and nitrous oxide

measurements. *Journal of Geophysical Research*, *112*, D24S36, https://doi.org/10.1029/2007JD008724

Pitts, M. C., Poole, L. R., & Gonzalez, R. (2018). Polar stratospheric cloud climatology based on CALIPSO spaceborne lidar measurements. *Atmospheric Chemistry and Physics*, *18*, 10881-10913, https://doi.org/10.5194/acp-18-10881-2018

Santee, M. L., Read, W. G., Livesey, N. J., Cofield, R. E., Cuddy, D. T., Daffer, W. H., Drouin, B. J., Froidevaux, L., Fuller, R. A., Jarnot, R. F., Knosp, B. W., Manney, G. L., Perun, V. S., Snyder, W. V., Stek, P. C., Thurstans, R. P., Wagner, P. A., Waters, J. W., Muscari, G., deZafra, R. L., Dibb, J. E., Fahey, D. W., Popp, P. J., Marcy, T. P., Jucks, K. W., Toon, G. C., Stachnik, R. A., Bernath, P. F., Boone, C. D., Walker, K. A., Urban, J., & Murtagh, D. (2007). Validation of the Aura Microwave Limb Sounder HNO_3 measurements. *Journal of Geophysical Research*, *112*, D24S40, https://doi.org/10.1029/2007JD008721

Solomon, S. (1999). Stratospheric ozone depletion: A review of concepts and history. *Reviews of Geophysics*, *37*, 275-316, https://doi.org/10.1029/1999RG900008

Waugh, D. W., Sobel, A. H., & Polvani, L. M. (2017). What is the polar vortex and how does it influence weather. *Bulletin American Meteorological Society*, *98*, 37-44, https://doi.org/10.1175/BAMS-D-15-00212.1

Zhang, J., Tian, W., Chipperfield, M., Xie, F., & Huang, J. (2016). Persistent shift of the Arctic polar vortex towards the Eurasian continent in recent decades. *Nature Climate Change*, *6*, 1094-1099, https://doi.org/10.1038/nclimate3136